Comprehensive characterisation of the compressive behaviour of hydrogels using a new modelling procedure and redefining compression testing

Jairan Nafar Dastgerdi*[a,b†], Janne T. Koivisto[c,d†], Olli Orell[e], Pantea Rava[f] ,Jarno Jokinen[e], Mikko Kanerva[e], and Minna Kellomäki[c]

[a] Department of Aerospace Engineering, Amirkabir University of Technology, 424 Hafez Avenue, Tehran, Iran.

[b] Department of Mechanical Engineering, School of Engineering, Aalto University, P.O. Box 14300, 00076 Aalto, Finland.

[c] Laboratory of Biomaterials and Tissue Engineering, Faculty of Medicine and Health Technology, Tampere University, Korkeakoulunkatu 3, 33720 Tampere, Finland.

[d] Division of Pathology, Department of Laboratory Medicine, Karolinska Institutet, Alfred Nobels allé 8, 14152 Huddinge, Sweden.

[e] Laboratory of Materials Science, Faculty of Engineering and Natural Sciences, Tampere University, Korkeakoulunkatu 6, 33720 Tampere, Finland.

[f] Department of Industrial and Management Engineering, Amirkabir University of Technology, 424 Hafez Avenue, Tehran, Iran.

† Authors contributed equally.

Email: Jairan.nafardastgerdi@aalto.fi

Abstract

The aim of tissue engineering is the regeneration of damaged tissue or the production of representative tissue organoids *in vitro*. To achieve this, one approach is to use hydrogels, water-swollen hydrophilic and crosslinked polymer networks, that can accommodate encapsulation of living cells and help the regeneration process. Even though mechanically biomimicking target tissue is important for a favorable cell response, the mechanical characterisation of tissues or hydrogels is not yet a fully defined process with various possible models and methods existing. In this paper, for the first time, a specific procedure and model has been suggested for the discussion of the nonlinear stress-strain relationship in large

deformations of hydrogels. Moreover, this approach has comprehensively characterised the compressive material performance of hydrogels in a theoretical framework. To present the performance and utility of the introduced procedure, it is used with two different compositions of bioamine crosslinked gellan gum hydrogel. In addition, a three-dimensional digital image correlation technique has been utilized together with compression testing to measure the actual force and deformation in unconfined compression. The material model parameters were obtained to represent nonlinear stress-strain behavior and the viscoelastic response (relaxation) of gellan gum hydrogel in compression.

Keywords: Compression testing, Hydrogel, Gellan gum, Mechanical properties, Viscoelastic deformation

1. Introduction

Hydrogels are three-dimensional (3D), water-filled, crosslinked networks of hydrophilic polymers [1,2]. Similar to the natural extracellular matrix (ECM), hydrogels are soft biomaterials that can contain biofunctionalisation sites for the attachment, migration and differentiation of cells. Moreover, hydrogels are currently being employed and explored for a broad range of medical applications, including cell encapsulation, drug delivery and tissue engineering (TE) [2-5]. In TE, the main goal is to combine a biomaterial, such as a hydrogel, with living cells to produce a piece of tissue *in vitro* that functions the same way as natural tissue *in vivo* [5,6]. The tissue can then be used in either therapeutic clinical applications to replace damaged or malfunctioning tissue [6] or as a model when studying developmental biology, disease modelling or toxicology *in vitro* [7,8].

Biomimicking the ECM mechanically is important in clinical TE as well as during modelling *in vitro*, as cells are known to respond to mechanical cues in their environment via mechanotransduction [8-11]. Thus, a good starting point for rationally designing novel biomaterials for TE is to make their mechanical properties match the target tissue [12]. While recent studies [13-17] have powerfully illustrated the role of mechanics in cell biology, the ECMs in tissues are not just linear elastic, and the high degree of nonlinearity in the stress-strain

relationship of ECMs and hydrogels as synthetic ECMs has been proven [18,19]. Hydrogels on their own are complex, hydrophilic polymer networks containing a large amount of water (over 95%), which makes hydrogels solids with strong fluid-type behaviour. Therefore, an important challenge is to determine how time-dependent and nonlinear mechanics regulate cell behaviours. In recent years, an increasing amount of effort has been devoted to the constitutive models of materials to accurately predict the comprehensive 3D stress-strain state [20]. The work-conjugate pair of logarithmic strain and Cauchy stress can even be determined over the large-strain region [21-24]. Numerous measurement techniques and setups, such as compressive (confined and unconfined), tensile, shear, indentation (macro- and micro-) and tests by rheometers, have been applied to validate models. However, the different output data from tests are not directly comparable to each other, especially in the case of anisotropic materials [25]. Furthermore, the test output can hardly ever be directly used to validate a material model – the effects of the shape of the test specimen, the contact to the test machine and the exact 3D deformation can be difficult to simply omit. Only recently has full-field data of the deformation become available. The 3D digital image correlation (3D-DIC) technique has become a widely used method to study full-field displacements and strains in numerous applications [26-27]. For example, in the area of biomechanics, DIC offers new approaches to study the behaviour of soft, sensitive and commonly anisotropic materials in various environments [28].

1.1 Elastic region

The applications of the concepts of the linear theory of elasticity [19,29] to a highly nonlinear material has led to the inevitable challenge of defining the limit between the elastic and non-elastic regions. Whenever a material, such as a hydrogel, expresses a significant effect by the loading rate (in detail strain rate) on the mechanical response, it will have to be modelled by the time-dependent response to stress [25, 30-32].

The existing literature on hydrogel mechanics is filled extensively with experimental research. Bai et al. [33] compiled a comprehensive list of the published, observed phenomena including solid mechanics, fracture mechanics and fatigue. According to numerous studies, it is

rather evident that hydrogel behaviour – including fracture onset, crack propagation and mechanical damage – is strain-rate dependent, and this dependence is a 'function' of the exact chemical composition. Hydrogels can significantly heal after ultimate phenomena (e.g., crack or crease onset), and this feature does not make it any easier to model the ultimate behaviour of hydrogels in a common manner.

The elastic region covers the behaviour where all strain energy stored in the body of the hydrogel (by external loading) can be recovered. Within the recovery of strain energy to another form (mainly potential energy), the body returns to its original state. For typical engineering materials, this type of behaviour occurs at relatively small deformations – within a magnitude of percent strain or less. For hydrogels, the reported 'elastic region', in terms of the percentage of specimen height compressed, ranges up to 10% [34]. However, hardly ever is the presumed elastic region verified in the current literature. Furthermore, the challenges in the test machine's crosshead-integrated sensor data are that it is not directly related to an elastic (nonlinearity) limit such as the true strain or stress level of a material model. The most common test to study the elastic and dissipative ranges of deformation is dynamic mechanical analysis (DMA). For hydrogels, the typical test sequence is run at a constant frequency and low deformation range (≈1% of specimen height) and with a load ratio of 0.1 [35]. Further frequency sweeps (0.1 Hz to 100 Hz) are run to determine the complex modulus [36]. Another alternative is small-amplitude oscillatory shear testing [35]. It should be noted, however, that a dynamic stiffness (storage modulus) does not correspond to the quasi-static elastic (Young's) modulus – especially for hydrogels, as noted by Kocen et al. [35].

The elastic region, per experimental actions, is highly dependent on the test speed [37]. Gofman and Buyanov [38] reported an unusual disappearance of hysteresis, yet they did not report permanent deformation. In their tests, hysteresis suggests either stress sign-dependent nonlinear elastic behaviour or relaxation-creep that is able to heal upon a single load cycle. Several studies (e.g., Nakamura et al. [37]) have shown that for constant hydrogel composition and test specimen geometry, an 'overly high' test speed and likewise an 'overly low' test speed leads to

simply non-linear behaviour (in force-displacement data). At an 'intermediate' speed, the behaviour tends to involve a linear region, although it might simply form a balance between the relaxation and strain-hardening effects in the specimen. At very low (i.e., 0.05%/min) test speeds, hydrogels begin to seep the internal solvent [39-45]. Hence, several modelling studies have dealt with poroelasticity and viscoelasticity separately [45-51], while only a few studies have analysed the combined poroviscoelastic models [32,52-54]. These models aim to phenomenologically describe the conformational change of the molecular network and the migration of the incompressible solvent [25,39]. Researchers have suggested that the elastic region of hydrogels could refer to the behaviour where solvent does not have enough time to migrate in a gel and when the poroelastic-type behaviour caused by the 'long-range' motion of (solvent) molecules is negligible [37,55-56].

1.2 Compressive testing of hydrogels

Compressive testing has the advantage of being relatively easy to perform in practice by using a universal tester, and the test data (force-displacement curves) are considered to be simple to interpret. Many researchers have interpreted test data as a direct uniaxial response of hydrogel bulk (material). Consequently, the suggested models mostly cover one and two-dimensional forms [52,54-55]. On the other hand, compression testing and the theory (of elastic response) has several challenging issues, such as exact changes of volume, as reported by Zhang et al. [76].

The typical reported crosshead displacement ranges of compression extend up to 60% of specimen height. Sometimes researchers have indicated the elastic region based on the initial 'instant fit' (tangent) to the engineering stress-strain derived from the crosshead displacement curve [35]. For reliable test data, the first data points are in a way problematic due to the load cell's inaccuracy and noise as well as the effects of non-ideal surface flatness. Some researchers suggested that Young's modulus could be directly calculated as a linear fit along the engineering stress-strain curve (derived from crosshead displacement) between 5% and 10% strain [34]. However, true stress or strain are hardly ever reported, and engineering stress and averaged

strain (namely, applied strain [57] from the crosshead displacement) or even normalized values are reported instead [36]. At these typical high levels of deformation, the test specimen behaviour cannot be presumed to be purely elastic. Therefore, since hydrogels contain mostly water, they are incompressible for any reasonable test procedure. For compressive deformations as high as 15% to 30%, the test specimen must significantly deform in the lateral direction to preserve the volume (Poisson's ratio ≈0.5). Ideally, when the test machine's (anvil) contact with the hydrogel is frictionless, the Poisson's effect is no longer a problem. However, when the contact friction goes to zero, the side force to slide the specimen out goes to zero. In practice, researchers use thin pieces of paper to increase the friction and to hold the hydrogel test specimen firmly in place [37]. The higher the friction, the more the hydrogel must worm (including local rotation) on contact with the test machine. Moreover, the shorter (low height to diameter ratio) the test specimen is, the more extensive are the contact-related effects on the test output data. On the other hand, a higher specimen easily bends and even buckles under the compressive load.

Due to the variety of hydrogel chemistry, the complex strain-rate dependence and the viscous-porous behaviour, it is anticipated that completely generalised test guidelines for an 'elastic region' and negligible nonlinearities as well as the contact effects cannot be given. However, a clear procedure should be established to investigate the significance of these 'artefacts' during the compressive testing of hydrogels and to determine the appropriate elastic region per hydrogel. Bai et al. [33] aimed to connect chemists and mechanicians – the next step is to define common, quantitative understanding.

1.3 Prerequisites

The lower bound of the compression test speed is not useful for determining the mechanics of hydrogels because the seeping or vaporizing of solvent results in something other than the original hydrogel, even anisotropy (gradients). For the upper bound, viscoelasticity governs hydrogel behaviour up to the deformation rate where the viscous flow or relaxation becomes negligible. It has been suggested that the viscoelastic region resembles reversible crosslinks in

hydrogels [30-32]. Combined spring and dashpot models are common for viscoelastic models in general. When these elements are connected in series, they are referred to as a Maxwell model, whereas a connection made in parallel is referred to as a Kelvin–Voigt model. In addition, specialised combinations are used for specific loadings and materials [58]. To determine the precise material constants for viscoelastic behaviour, further testing is required, yet this testing can be performed by applying compression. In summary, a reasonable procedure for the compression testing of hydrogels to determine compressive (Young's) modulus must contain the following elements:

I. Tests run at several test speeds (strain rates)

II. Tests run over a displacement range without observable permanent damage (e.g., crease [57])

III. Accurate analysis of linearity per test speed using fitted viscoelastic models

IV. An iterative scheme for estimating the significance of viscous effects over a truncated displacement range with selected acceptable error

V. Finite element analysis to estimate the significance of test artefacts at test machine-hydrogel contact with DIC comparison

VI. Correcting for relaxation to resolve the value of compressive modulus

The hydrogel type chosen in this study for the characterisation of mechanical behaviour, the testing of a new mechanical model and the characterising approach is gellan gum (GG) [59], a bacterial polysaccharide with high potential for TE applications and 3D cell culturing [60-62]. The bioamine crosslinking of GG [60] and the chemical crosslinking of oxidized GG with hydrazide-modified hyaluronic acid [61] and hydrazide-modified gelatin [62] via hydrazone reaction, have been reported by some authors to be potential methods for the production of biocompatible hydrogel for soft TE applications. When using the bioamine GG in neuronal cell culture, it was noted that the neural cells prefer a surprisingly high elastic modulus (≈23 kPa) compared with our reference measurements with brain tissue (≈7-10 kPa) and common published results (<1 kPa) [9,60]. A possible reason for this discrepancy is the inadequacy of

the mechanical model and the test procedures. Therefore, an extensive analysis of the compression testing for hydrogels is presented to determine the appropriate elastic region in the following study.

2. Experimental

2.1. Preparation of hydrogel

Gellan gum (GG, Gelzan™, low acyl, Mw 1 000 g/mol), spermine tetrahydrochloride (SPM) and sucrose were obtained from Sigma-Aldrich (St. Louis, MO, USA) with the highest level of purity available. The hydrogel solutions were prepared as previously stated and followed the same protocol as used in cell culture experiments [60]. In brief, 10 % (w/w) sucrose in deionized water was used as solvent; GG was dissolved at 5 mg/ml and SPM at 0.35 mg/ml and at 0.175 mg/ml. After dissolution, all solutions were sterile filtered at 60 °C with a 0.8/0.2 µm Acrodisc® syringe filter (PALL Corporation, Port Washington, NY, USA). To produce a compression sample, solutions were heated to 37 °C in a water bath. The SPM crosslinker was combined with GG at a volume ratio of 4:25 and mixed with a magnetic stirrer as described in [63], and cast into self-made cylindrical moulds with an approximate height of 6.5 mm and a cross-sectional diameter of 12.2 mm. The specimens for testing were incubated overnight in a humid atmosphere at 37 °C and tested the following day. In this study, two different SPM crosslinker concentrations, 1.1% and 0.6% (w/w of polymer), were tested. These concentrations, chosen based on our previous study [60], were found to be mechanically biomimicking to soft tissue and suitable for 3D cell culture applications.

2.2. Compression testing

Unconfined compression testing was performed with a Bose Electroforce BioDynamic 5100 machine using WinTest 4.1 software and 225 N load cell (TA Instruments, Eden Prairie, MN, USA). Due to the softness of 0.6% SPM hydrogel, the load cell was changed to 22 N (TA Instruments), and digital filtration at 1 Hz was used to reduce the noise in the load signal. The compression test parameters (displacement rate, starting point, friction) were varied to gain a

complete view of the hydrogel's viscoelastic response, and a part of the individual tests were analysed using a 3D-DIC setup as described in the following section. All tests were performed on wet hydrogels at room temperature. In addition, a wetted piece of lint-free cellulose paper (Cellulose wadding, Katrin, Espoo, Finland) was used on both compression plate surfaces to increase the friction between the hydrogel and the test machine boundary as well as to prevent sample slippage. The exact dimensions (diameter, height) of each sample were measured with callipers before testing. The standard test parameters were the same as in [60], [63], compressing the sample at different displacement rates until reaching 65% displacement of the original sample height (causing fracture). In this study, 10 mm/min and 1 mm/min displacement rates were examined to observe the rate dependency of the hydrogel compression.

2.3. Digital image correlation

The 3D-DIC technique [27] using lenses with a focal length of 100 mm was used to study the surface deformations during the compression tests of the hydrogel samples (Fig. 1). Using this technique, the unique features of the sample surface are recorded simultaneously by two cameras (5 Mpix Imager E-Lite, LaVision, Germany).

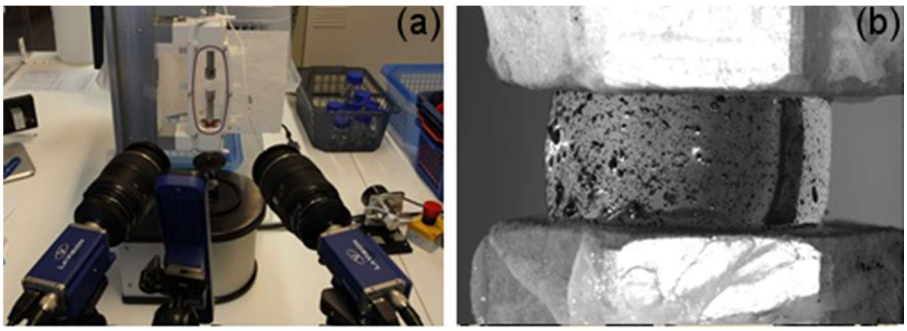

Fig. 1. (a) The 3D-DIC test set up, (b) an image taken of a sample with carbon black speckle pattern.

From the recorded images, the full-field surface deformation map was obtained by tracking the movement of the surface divided into small subsets. The unique surface pattern required for the carrying out of the experiments was accomplished by blowing fine carbon black powder (Corax® N550, Evonik, Germany) on the naturally transparent, moist sample.

The lighting of the sample was performed using two synchronized pulsed led lights operated directly via DIC software (Davis 8.4, LaVision). To achieve a constant and flat light throughout

the sample, the reflections caused by the curved, wet and transparent sample needed to be optimised and balanced. The recording rate of the 3D-DIC measurements ranged from 1 Hz to 8 Hz, depending on the total time per each compression test. The scale factor of the images was 8 µm/pix, and the root mean square (RMS) fit of the calibration was 0.4 pix.

The deformation analysis was performed using Davis 8.4 software. The used subset and step sizes were 55 pix × 55 pix and 15 pix, respectively. To ease the tracking process against, e.g., an artificially changing pattern due to seeping water on the surface or changing reflections due to curvature changes of the sample surface, the applied correlation mode in the analysis was the sum of differential images instead of the more conventionally used mode (i.e., relative to the first image). In addition to the qualitative examinations of the sample deformations, axial surface strains and radial surface displacements were calculated from the correlation results.

3. Theory/Calculations

3.1. Determination of stress and strain

Due to the finite but complex deformation [81] of the test specimens, logarithmic strain (ε^{n}), and Cauchy stress (σ^{c}) are employed in this study. The logarithmic strain possesses certain intrinsic properties that show its favoured position among all strain measures [22,81]. In the uniaxial case, to start with, the Cauchy stress takes the following form:

$$\sigma^{c} = \frac{N}{A}, \tag{1}$$

where (N) is the applied force, and (A) is the true, current cross-sectional area.

The logarithmic strain is defined as follows:

$$\varepsilon^{n} := \int_{l_0}^{l} \frac{\mathrm{d}l}{l} = \ln\frac{l}{l_0}\ , \tag{2}$$

where (l_0) and (l) are the initial and current gauge length of the sample, respectively. Here, the positive directions are defined so that the strain for tensile deformation is positive and, likewise, stress for tensile loading is positive. After mathematical manipulations, the logarithmic strain

and the Cauchy stress are obtained in terms of engineering strain (ε^{eng}) and engineering stress (σ^{eng}) as follows:

$$\varepsilon^{n} = \ln(1+\varepsilon^{eng}) \tag{3}$$

and

$$\sigma^{c} = \sigma^{eng}(1+\varepsilon^{eng}). \tag{4}$$

3.2. Uniaxial approximation for the analysis of linear region

A mathematical model has been presented to characterise the presumed nonlinear (elastic) mechanical behaviour of hydrogels covering the possible toe region followed by a continuous elastic behaviour [58,64]:

$$\sigma = \begin{cases} A(e^{B\varepsilon}-1) & \forall\, \varepsilon \le p \\ E(\varepsilon - p)+q & \forall\, \varepsilon \succ p \end{cases}, \tag{5}$$

where (σ) is the stress and (ε) is the strain. This nonlinear fitting simultaneously applies the modulus (E), transition strain (p) and transition stress (q) where the transition point is defined as the end of the initial toe region (if a toe region is observed). At the transition point, the stress-strain curve shifts from strain-stiffening to strain-softening.

To maintain the elastic modulus (E), the slope of the linear portion was defined as the slope of the stress-strain curve at the transition point (p,q) between the two portions. Thus, this equation can be fully defined by three parameters: p and the constants A and B. Using the MATLAB function *fmincon*, the parameter values (A, B and p) are simultaneously optimised to minimise the mean square error. It should be noted that the optimisation here is performed on the entire selected data, simultaneously fitting the exponential section and the linear section, and that the location of the transition point is a continuous variable included in the optimisation process. This approach maintains continuity at the transition between the exponential and linear portions of the stress-strain curve.

3.2. Relaxation test and data analysis

In general terms, a viscoelastic material shows the behaviour of both an elastic solid ($\sigma = E\varepsilon$) and a viscous liquid ($\sigma = \eta\dot{\varepsilon}$) at the same time when subjected to a stress or strain. A commonly used test to measure the viscoelastic properties of hydrogels is the stress relaxation test. In this test, a constant strain (ε_0) is targeted by applying constant crosshead displacement, and the reaction force at the test machine is recorded over time. Within the terminology of statistical mechanics, relaxation means an irreversible process in contradistinction to the time-reversible process of Newtonian mechanics. It is the change of a system from one physical state to another, involving the dissipation of energy. Relaxation is generally described by the following function:

$$\sigma(t) = \sigma_\infty + \sigma_0 G(t), \tag{6}$$

where (σ_∞) and (σ_0) are material constants, and $G(t)$ is the normalized relaxation function [65-66]. The best known relaxation function is the simple exponential decay function:

$$G(t) = \exp(-\frac{t}{\tau}), \tag{7}$$

where (τ) is the relaxation time. This parameter determines the rate of decrease of the relaxation function. It is well known that Eq. (7) is the solution of the linear first order equation:

$$\frac{d\sigma}{dt} = -\frac{1}{\tau}(\sigma(t) - \sigma_\infty). \tag{8}$$

It means that the rate (of approximation) of the parameter to the equilibrium state is proportional to its shift from the equilibrium state. Wide-ranging experimental information leads to the conclusion that pure exponential relaxation is rarely found in nature [67]. To describe the relaxation that does not obey the simple exponential law, the empirical stretched exponential law or the Kohlrausch-Williams-Watts (KWW) function has been widely applied [68-69]:

$$G(t) = \exp(-\frac{t}{\tau})^\beta, \tag{9}$$

where β is an empirical exponent ($0 \le \beta \le 1$). The β term in the KWW stretched-exponential characterises the degree of non-exponentiality of the relaxation function.

The main difference between exponential decay and KWW-type relaxations is the nonlinear dissipation of energy. A non-linear behaviour in the stress relaxation response of the hydrogels has been predicted using KWW-type relaxation.

The time dependent relaxation modulus of the material is defined as:

$$E_{rel}(t)=\frac{\sigma(t)}{\varepsilon_0}. \tag{10}$$

At the beginning of a stress relaxation test, the test specimen is loaded suddenly and, by definition, so fast that only elastic deformation can take place (i.e., a test rate to iterate per hydrogel chemistry). It is convenient to set the zero-reference for time to this moment. Therefore, the strain is given at $t=0$ as ε_0 can be calculated by presuming Hooke's law as follows:

$$\varepsilon_0=\frac{\sigma_{11}^c}{E} \quad where \quad \sigma_{11}^c=\frac{N}{A}. \tag{11}$$

Similar to the above, in Eq. (11), the variable N is the measured force and A is the current cross-sectional area of the sample. E is the linear region modulus (for a selected or truncated single linear portion model of the elastic region). Finite element implementations can be made by using a series expansion of the relaxation modulus (see Section 3.3.).

3.3. Test artefacts, 3-D effects and strain rate effects for test data truncation

The effects of the true 3D stress-strain field, the contact with the test machine, and possible specimen inhomogeneity must be in details analysed. Here, ABAQUS (Standard and Explicit) code was used for the simulations in an axisymmetric space. The test machine surfaces were modelled as analytical rigid. As a starting point, the bulk hydrogel specimen (height 6.5 mm, radius 6.1 mm) was connected in a rigid manner (i.e., tie constraint) to the machine. Then, elastic moduli of 15.36 kPa and 1.719 kPa were studied one by one (based on Fig. 10b), and a Poisson's ratio of 0.48 (nearly incompressible) was applied. The bulk hydrogel was meshed using the fully-integrated biquadratic quadrilateral elements (CAX8). As an explanation for the formation of a toe region in some experiments (shown by force-displacement data), anisotropic elastic behaviour was studied as an alternative – the engineering constants are derived in the Appendix.

Similarly, an inhomogeneous hydrogel specimen was considered by modelling a 'skin' (100 μm by partition), forming the free surface of hydrogel having the higher modulus of the two above values. The skin formation in reality could follow the vaporisation of solvent on the free surfaces. Also, a membrane-like skin (a type of behaviour) was studied by using quadratic membrane elements (MAX2) with a given thickness of 10 μm (modulus 15.36 kPa, Poisson's ratio of 0). The interface between the membrane-like skin and bulk was a frictionless non-penetrating contact formulation. For both skin simulation cases, an upper limit of 6 kPa was defined and followed by an ideal-plastic behaviour.

For a rigid machine-hydrogel contact, it was observed that the hydrogel specimen reached stresses beyond any reasonable strength at the very beginning of a compression test. Therefore, at the contact near the free edge of the specimen ('corner'), the hydrogel must either slide, worm and/or flow locally (via plastic or viscous flow). An enhanced contact was studied as an alternative by applying a penalty-based contact with a friction coefficient of 0.2. Additionally, a slight rounding (radius 0.5 mm) of the specimen corner was considered. For an artefact of the specimen's geometry, a convex sample top (5 °), i.e., non-flat contact to the test machine, was studied. The simulations were run by launching an enforced displacement in the direction of the symmetry axis (i.e., compression).

The dynamic effects and relaxation during compression testing (at displacement rates of 1 mm and 10 mm/min) were simulated using the explicit solver of ABAQUS. Pure linear elastic and viscoelastic material models were incorporated (rate-dependent time domain viscoelasticity). The viscoelastic part was inputted by using the relaxation test data, i.e., 600 experimental data points of the fitted $G(t)$ of Eq. (9) to create the Prony series parameters of the relaxation modulus. The elastic deformation was based on elastic modulus (values 15.36 kPa and 1.719 kPa were analysed one by one). The elastic modulus was defined as instantaneous stiffness so that a Maxwell-type coupling with viscous dissipation is produced for the simulated tests. A density of 1000 kg/m^3 was used for the hydrogel. Mass scaling of ×100 was used, and a survey was made to check the effects for up to ×1000 scaling. The quadratic triangle element (CAX6M)

was used for the explicit computations. The FEA models included 3656-9452 variables for the different simulation cases.

4. Results and discussion

4.1. Measured compressive behaviour of hydrogel

Fig. 2 shows typical Cauchy stress-logarithmic strain curves of GG hydrogel specimens for two different test speeds. The displacement rate-dependent stress-strain behaviour of the hydrogel samples can be clearly observed in this graph. For a low displacement rate, the stress state relaxes during the test and leads to a lower peak stress level.

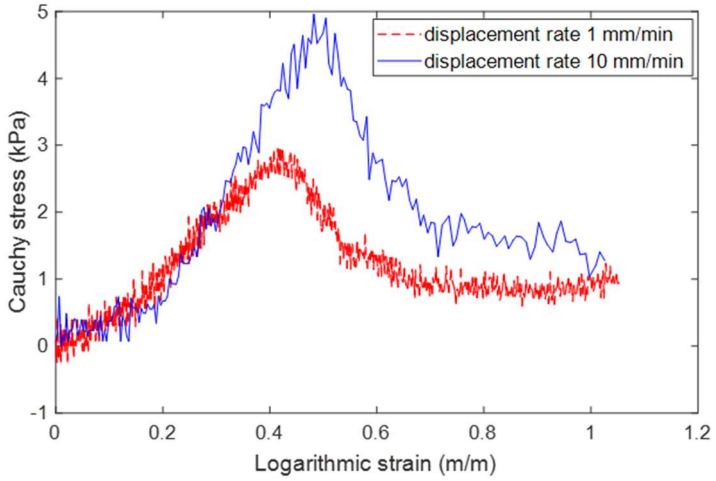

Fig. 2. Typical examples of the Cauchy stress-logarithmic strain curves for the bioamine crosslinked GG hydrogel (1.1% SPM). Test results at two different displacement rates are given.

DIC has previously been applied to studying the compression behaviour of bioactive-glass-reinforced GG with both visible light and micro-CT imaging, but only to freeze-dried scaffolds [70, 71]. To our knowledge, DIC has not previously been used on wet GG hydrogels. Here, visible light DIC has been used during the unconfined compression of wet hydrogels. In Fig. 3a, a full-field strain map of the axial strains in the sample tested with a test speed of 10 mm/min is presented. Near the compression plates, the strain field is strongly uneven, which mostly arises from DIC subset-related issues close to the interface between the rigid (compression plate) and the deforming (specimen) surfaces. Based on the full-field data, the nominal axial strains were

calculated using a virtual strain gauge size of 1.5 mm x 1.5 mm located at the centre of the sample (from which a mean strain value was calculated).

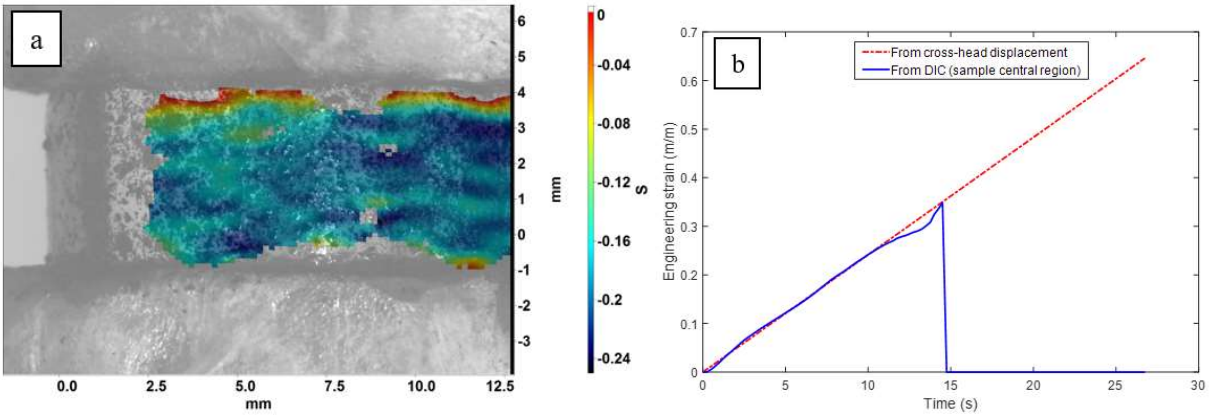

Fig. 3. (a) Strains in the loading direction ε_{yy} at sample surface after 8 s. (b) Comparison of the determined engineering strains. Displacement rate was 10 mm/min.

In Fig. 3b, the determined DIC strains are compared with the engineering strains calculated from the crosshead displacement data and a good correspondence can be seen. Furthermore, the correspondence indicates that the logarithmic strain calculated from the crosshead displacement data reliably represents the strains at the middle of the specimen. At a timestamp of 14.5 s, the fracture initiates in the specimen, which is seen as a sudden load drop in the recorded data and also from the recorded images (Supplementary Video 1). After the specimen fracture (14.5 s), the DIC correlation process fails in post-processing due to the rapidly changing surface pattern, and no further data from the DIC analysis is obtained. Fig. 4 depicts the determined radial surface deformation during a compression test using 3D-DIC measurement. It can be seen that the variation of the cross-sectional area of the specimen is significant. Clearly, simply-defined engineering stress and strain terms cannot illustrate the reality of this hydrogel material. Using 3D-DIC measurement and the radius change of the cross-section, the current cross-sectional area of the specimen and the true stress can be calculated. Thus, by using these data and considering hydrogel as an incompressible material with constant volume after deformation, the true strain can be obtained [72].

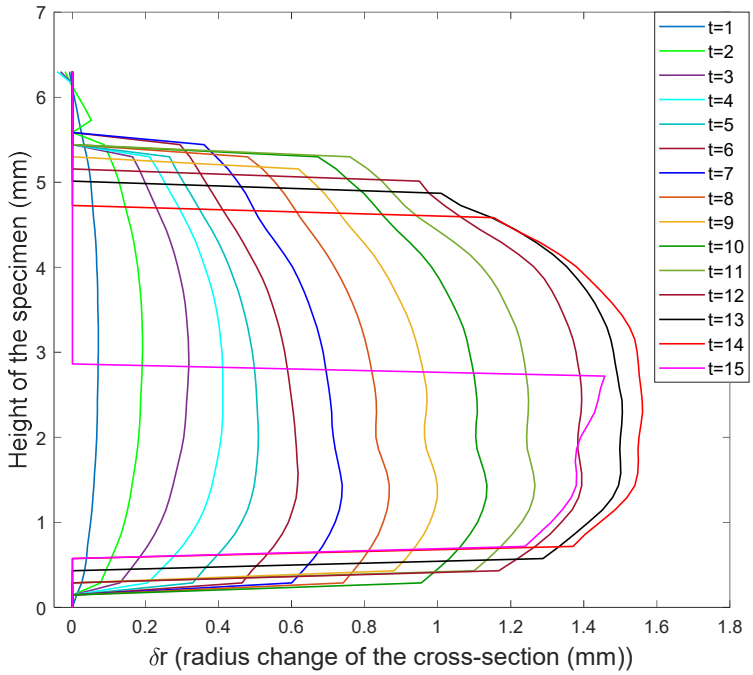

Fig. 4. The radial surface deformation of a typical hydrogel specimen during a compression test. The initial height of the sample is 6.3 mm.

The Cauchy stress–logarithmic strain curve obtained by applying experimental data and calculus in Eqs. (3) and (4) is shown in Fig. 5. The engineering stress-strain curve and the true stress-strain curve from the 3D-DIC measurement are illustrated. It can be seen that there is a significant difference between the engineering stress-strain curve and the two other curves (true stress-strain obtained from the 3D-DIC measurement and the Cauchy stress-logarithmic strain curve), whereas there is a good agreement between the true stress-strain curve from the 3D-DIC measurement and the Cauchy stress-logarithmic strain curve. Thus, the Cauchy stress and logarithmic strain have been used in the constitutive law to determine the material properties of hydrogel materials. However, most of the studies in this field have employed the engineering stress-strain curve to determine the mechanical properties of the hydrogels under tension or compression [29, 60, 73-75].

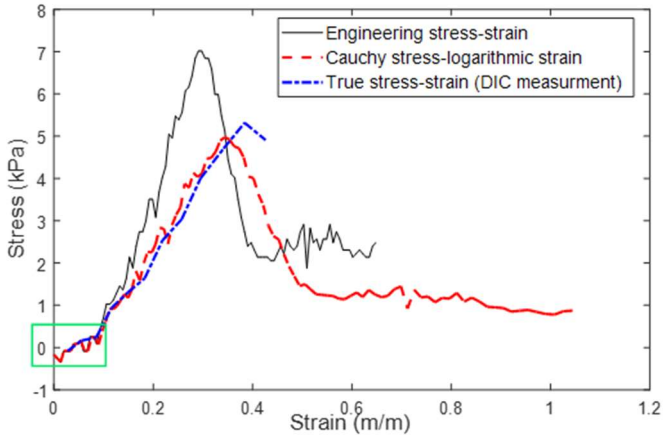

Fig. 5. Engineering stress-strain curve of a hydrogel specimen in comparison with the true stress-strain curve based on 3D-DIC measurement and the calculated Cauchy stress–logarithmic strain curve. The green rectangle highlights early phase of compression, where the strain increases, although the stress remains small. The displacement rate is 10 mm/min.

4.2 Frictional contact between hydrogel and anvil

In Fig. 5, it can be seen that at the beginning of loading, the strain increases, although stress takes very small values. This region is highlighted by a green rectangle in Fig.5. This region forms in the very early phase, and it is necessary to determine whether different boundary conditions could cause this behaviour as an artefact or as an actual material response. Here, various experimental measurement methodologies have been investigated to understand the early deformation phase. Therefore, a specimen was compressed without using a piece of paper between the sample and the compression plate (lowest friction case). In theory, a frictionless boundary would be ideal for compression testing [76].

Fig. 6a-b illustrates the Cauchy stress–logarithmic strain curves of two typical specimens under compression loading with and without the piece of paper when using a 10 mm/min displacement rate. Since the effect of the loading boundary condition was studied for the early phase, the target load level was approximately 50% of the fracture load level. The testing without the paper was only possible to ~30% of the displacement range, after which the specimen tended to slip off from between the compression plates due to low friction.

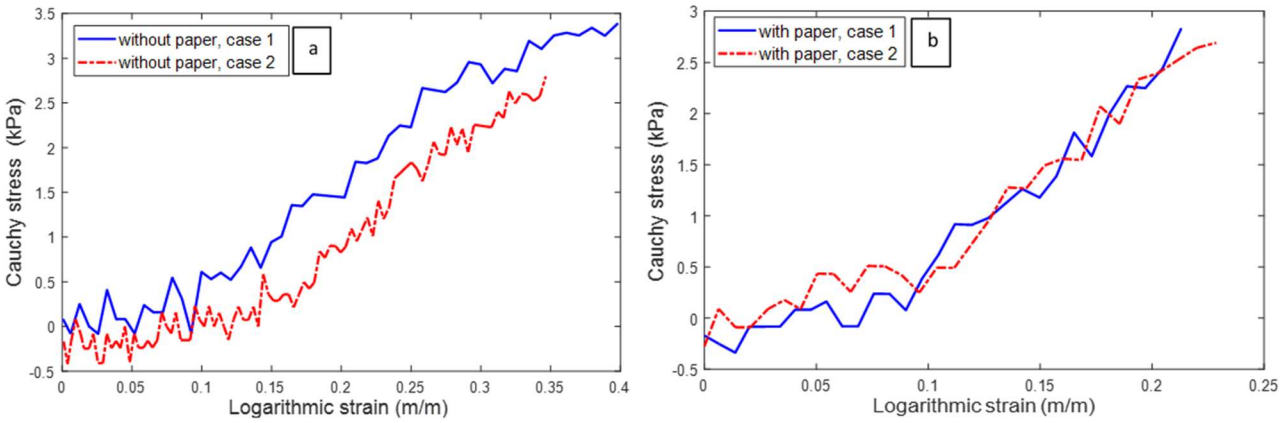

Fig. 6. The Cauchy stress–logarithmic strain curves of hydrogel specimens under compression loading (a) without and (b) with pieces of paper placed between the specimens and the test machine (compression plates).

Changing the paper between each specimen helped to keep the contact friction constant between tests, as the pores of the papers from previous tests were probably filled with hydrogel residue. Further varying of the friction between a specimen and the compression plate was carried out to study the boundary effect in detail. Fig. 7 shows the effect of the piece of paper at the specimen-machine boundary on the specimen form as the test proceeds. Here, the radial surface deformation along a vertical line on the specimen surface is obtained from the 3D-DIC measurements. The barrelling effect, i.e., the change in the specimen form sideways, is significant due to friction at the interface between the specimen and the compression plate. Moreover, it is also obvious that the simply defined engineering stress and strain cannot illustrate the real behaviour of the hydrogel specimen. The barrelling effect is more significant when new pieces of paper are used, but the deformation is essentially symmetrical. When the paper pieces are used several times for subsequent specimens, the changed friction at the specimen-machine interface, e.g., due to water/residues from the previous specimen or due to the damaged paper, causes the specimen to deform unevenly. Furthermore, when removing the old and installing the new specimen, the pieces of paper may easily fold in front of the specimen and cause obstacles to the optical axis of the cameras. If the whole specimen surface is not visible to both cameras used in the 3D-DIC, the correlation process cannot be carried out for those regions. In Supplementary Videos 2A-B and 3, cases of applying new and old pieces of

paper at the sample machine boundary are presented. However, the plain videos cannot fully cover the differences. Fig.7 provides more information about the boundary effects.

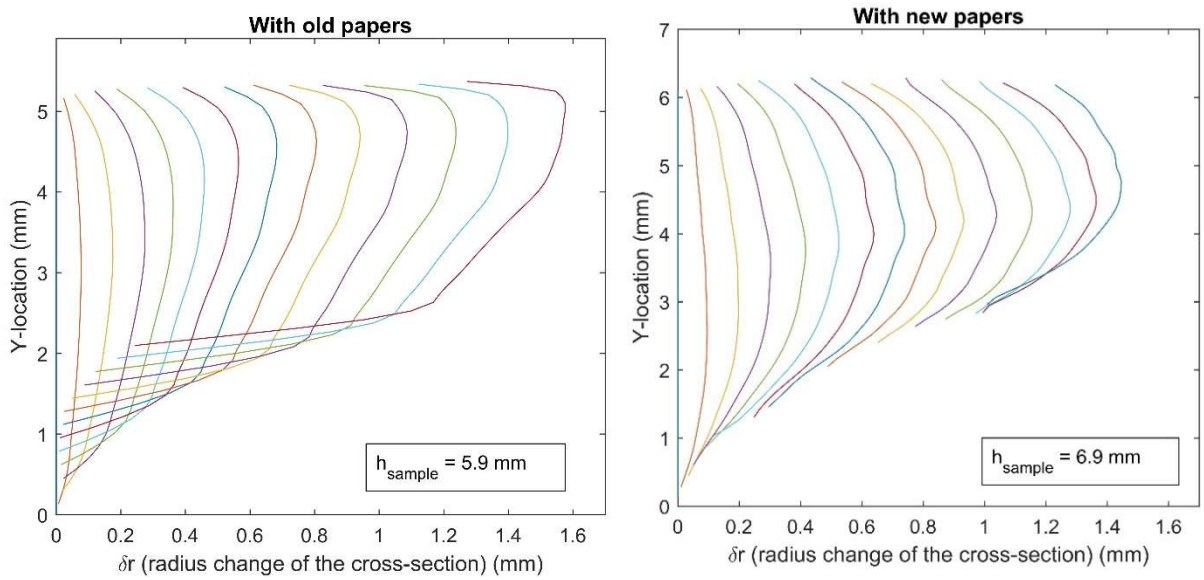

Fig. 7. The radial surface deformation for hydrogel specimen during compression testing and the effect of the pieces of paper placed between the specimen and test machine. The time interval between the curves in each figure is 1 s.

4.3 Threshold load and 'toe region'

The load threshold for defining the test start regarding the material response was examined. The compression was either pre-loaded so that the test machine indicated a 0.06 N pre-load, or the test was started above the hydrogel without any contact with the specimen surface. Only 1.1% SPM hydrogel was used for this determination of the measurement parameters step. Figs. 8 and 9 depict the Cauchy stress-logarithmic strain curves of two typical specimens in cases where the test started with a threshold of 0.06 N pre-load (Fig. 8) and above the specimen (Fig. 9). These different pre-loading conditions yield more information about the early phase and the response for low loads and small strains, indicating the existence of the so-called toe region in the stress-strain curve [29, 77].

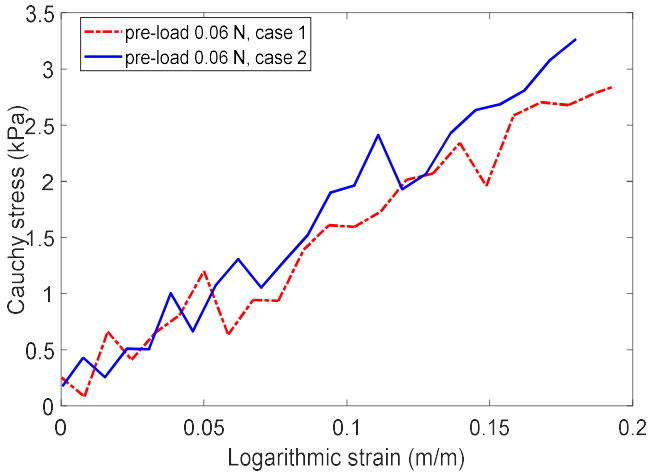

Fig. 8. The Cauchy stress-logarithmic strain curve of hydrogel specimens under compression loading with a 0.06 N pre-load. The displacement occuring during pre-loading of the specimens has been compensated in the strain.

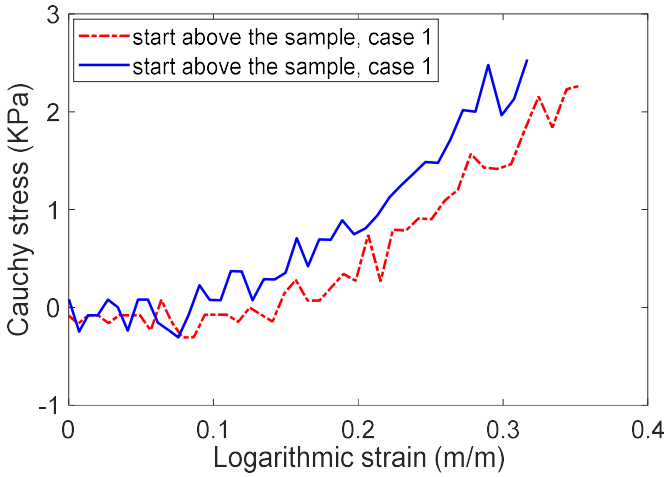

Fig. 9. The Cauchy stress–logarithmic strain curves of hydrogel specimens under compression loading, and then the test is started above the specimen without contact.

4.4. Linearity of data and test interpretation

Researchers have reported a non-linear region (toe region) at the beginning of the stress-strain curve of hydrogels [29,60,73,74,78]. In all the tested cases in these studies, the initial resistance of hydrogels against applied load and further deformation with increased load at specific strain has been observed. In this study, it is proposed to characterise the stress-strain behaviour of hydrogels, including an exponential toe region followed continuously by a linear elastic region (fitted per hydrogel composition). A continuous method is introduced to fit both the exponential and linear portions simultaneously, which ensures continuity between regions and the necessary accuracy. To highlight the efficiency and utility of the proposed approach, the performance of this method is compared to the more

conventional piecewise method [78]. Fig. 10a-b shows the characterized stress-strain curve of hydrogel compositions with 1.1% SPM concentration using the proposed approach and the conventional piecewise method. The values for parameters A, B, E, p and q are presented in Fig. 10a. To provide a better overview of the performance and efficiency of the proposed approach, the fully linear and nonlinear part of the model have been employed to present the material behaviour of hydrogels, as done by most researchers, applying a single full linear or a single full nonlinear approach (region) to the presented mechanical properties of hydrogels and biological materials [29, 60, 73, 74, 78].

In the conventional piecewise method, two different 'elastic moduli' are considered as a model to represent the elastic behaviour of hydrogel by fitting a linear curve to the toe and further elastic region of the stress–strain curve as shown in Fig. 10b. The first modulus (E_1) is proposed for the early nonlinear-elastic region (i.e., toe region) and the second modulus (E_2) is considered for the latter linear-elastic region. The strain range of the toe region was calculated by extrapolating the curve tangent of the linear portion of the stress–strain curve during the test to failure to the strain axis. The strain at which the curve crossed the strain axis was taken to be the strain range of the toe region [77]. Using a separate piecewise fitting method for each region, the two curves are independently fitted to a separate set of data points. It can be seen that the application of this method resulted in a discontinuity of 0.7 kPa at the transition between two regions. The magnitude of this discontinuity is large and clearly apparent for the experimental data used.

Even if the piecewise method developed the exponential curve for the toe region followed by a linear curve for the elastic region, there will be a discontinuity in the derivative of the stress-strain curve, leading to an inflection at the transition between two sections. Thus, there is no continuity in the performance of the piecewise technique at the transition between the two regions, leading to inaccuracies in the material model. However, the continuous method proposed in this study performs in continuity in both the stress-strain curve and its derivative by simultaneously optimising the curve fit for both regions. The continuous method has

provided an improved fit to the data, resulting in a more accurate material model for the hydrogels.

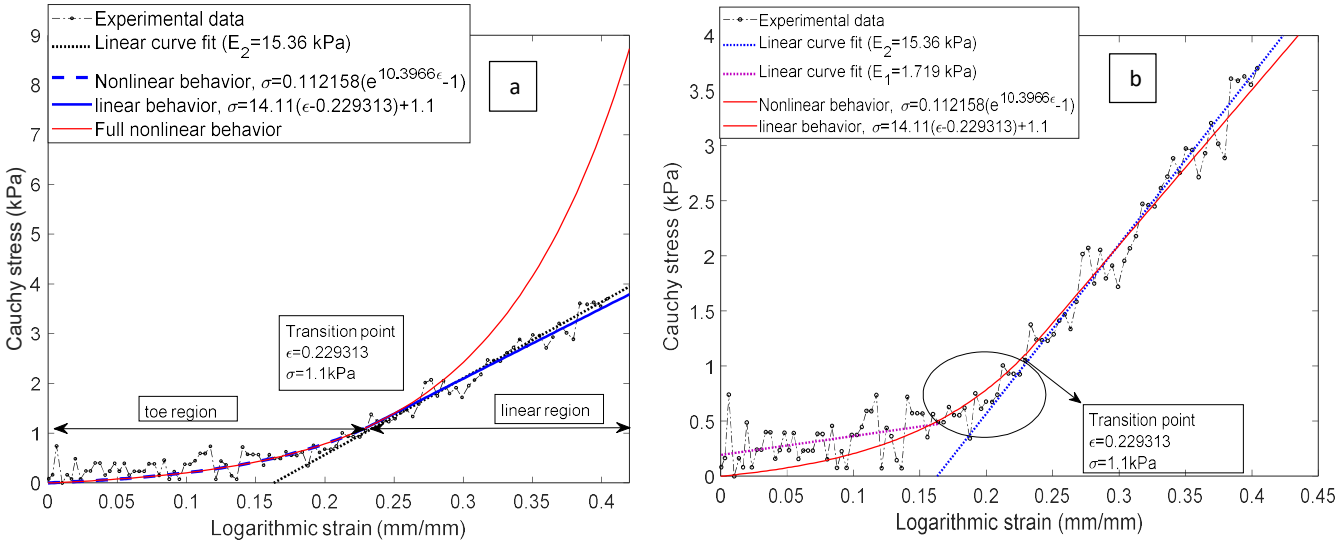

Fig. 10. Determination of the value of the model parameters for (performance of) (a) the proposed continuous method and (b) the piecewise method for 1.1% SPM concentration. The displacement rate is 10 mm/min.

To present the applicability of the proposed approach, the same analyses have been carried out for the other hydrogel compositions with 0.6% SPM concentration as depicted in Fig. 11a-b.

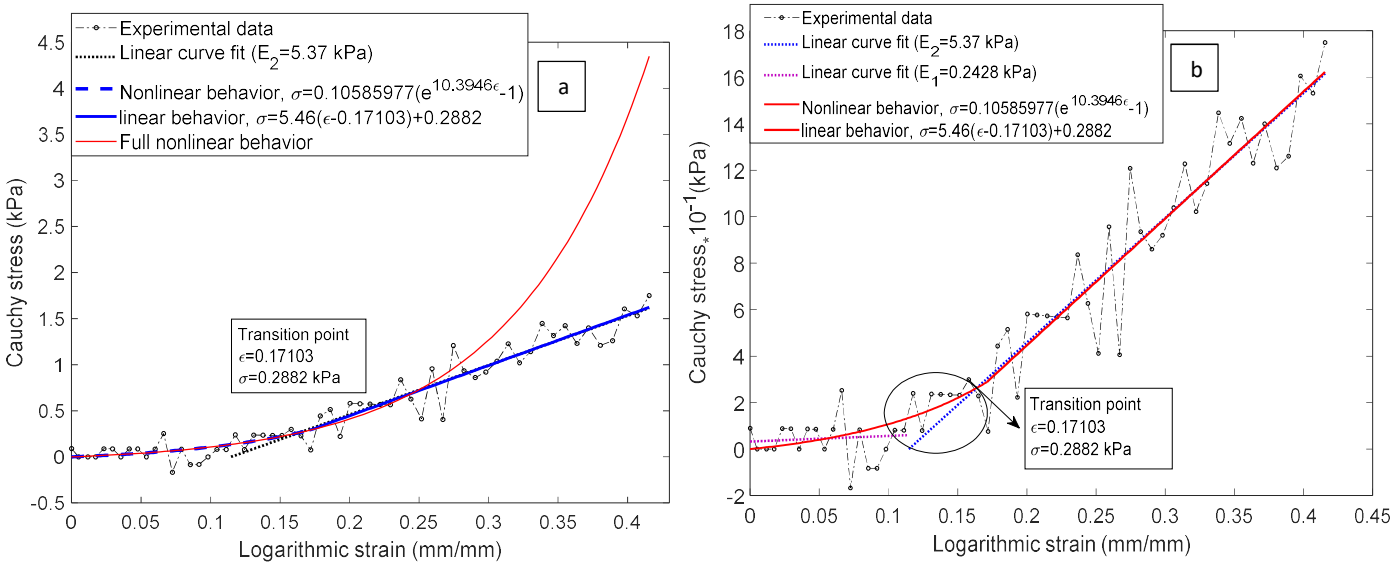

Fig. 11. Determination the value of the model parameters for (performance of) (a) the proposed continuous method and (b) the piecewise method for 0.6% SPM concentration. The displacement rate is 10 mm/min.

When comparing to soft tissue, the division of the stress-strain curve into the toe region and linear region is due to the elastin fibres of the ECM (carrying the stress initially) which, after a certain amount of strain, transfer the load-bearing to the collagen fibres (which only take the

load once they unfold [68,69]). This type of correspondence in terms of having similar toe and elastic regions in the hydrogel's stress-strain curve is a strong indication of the material's biomimicry, which is the desired property. Similarly, as in tissue, the unfolding molecules carry the initial load, and the crosslinks of the GG molecules begin carrying the larger portion of the load once they unfold. The molecular structures of collagen and GG are highly similar to each other, collagen forms a triple helix and GG a double helix, both via Coulombic forces [79, 80]. As the ionic crosslinking of GG stabilises the hydrogel network [80], the hydrogen-bonded helices give the materials this biomimicking behaviour. However, at longer strains, GG will exhibit brittle behaviour and fractures at much lower strains than collagen hydrogel or actual soft tissue. This is likely due to weaker bonds when compared to those between peptides in collagen, being only a double and not a triple helix, and missing the small composite enhancement effect of elastin fibres [19, 77-79]. Thus, the multi-portion elastic region and its model to describe the hydrogel can be considered biologically relevant and should be used whenever final results indicate this behaviour.

4.5 Stress-relaxation parametrisation

The stress-strain-time relationship, or constitutive law, can be determined by loading a hydrogel specimen at a constant load (referring to creep test) or a constant deformation (referring to stress relaxation test). In this study, the stress relaxation test is applied, and it is defined as a gradual decrease in reaction force (stress) with time under a constant deformation (strain level). At high strain rates, it has been observed for hydrogels that there is a time-dependent deformation and not much water seeps out during a test. Therefore, a viscoelastic material behaviour is proposed initially to approximate the behaviour of hydrogels. Here, a hydrogel specimen is suddenly deformed by compressing the specimen until a predetermined force (stress) level is reached, after which that displacement level is constantly maintained [81]. The load level consideration in this study is approximately 50% of the fracture load. The engineering stress versus time relation during the proposed relaxation test procedure is depicted in Fig. 12 for four typical specimens with 1.1% SPM concentration.

As explained in Section 3.1 and due to the finite deformation of the test specimens, the Cauchy stress (σ^c) was employed in this study. The Cauchy stress versus time relation during the proposed relaxation stress test procedure for one of typical specimens of 1.1% SPM concentration is depicted in Fig. 13.

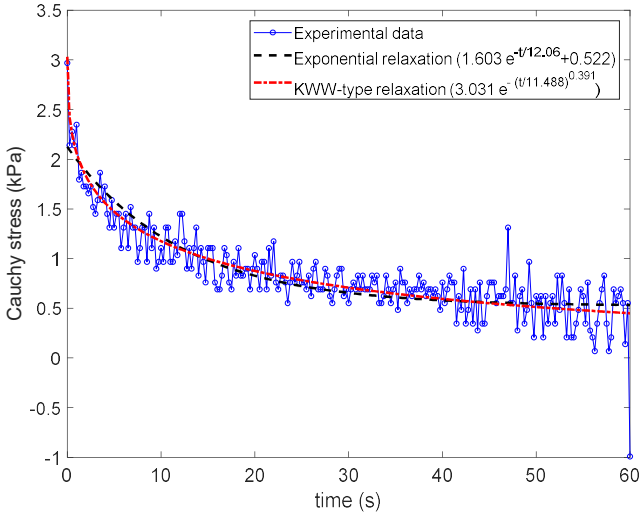

Fig. 12. The engineering stress versus time relation during the stress relaxation test for GG 1.1% SPM specimen.

The values for the material parameters (τ , β , σ_0, σ_∞) used in the simple decay exponential function and the stretched exponential KWW function, Eq. (6), can be obtained using a curve fitting technique. Fig. 13 also shows the data curves for the fitting and experimental reference. Using these values, it is possible to define relaxation modulus, Eq. (10) as a characteristic for stress relaxation behaviour.

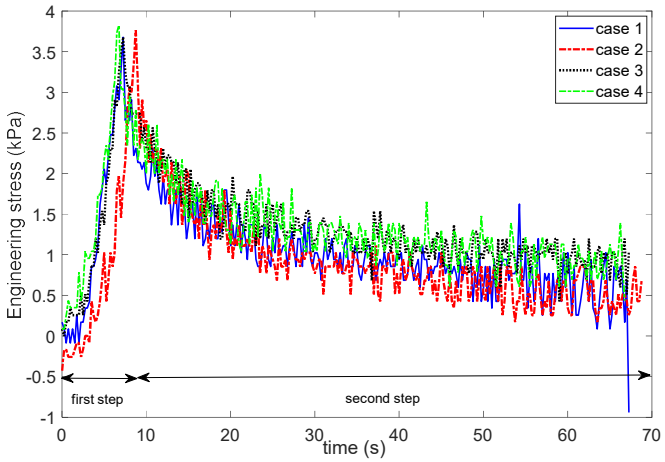

Fig. 13. The Cauchy stress versus time relation in the second step of the stress relaxation test of the GG 1.1% SPM specimen held in constant displacement for 60 seconds with the values for the material parameters (τ , β , σ_0 , σ_∞) employed in the simple decay exponential function and the stretched exponential KWW function. (225 N load cell in experiment)

The same procedure was carried out for the GG 0.6% SPM specimens. The Cauchy stress versus time of relaxation for one typical specimen of the other composition with 0.6% SPM concentration and the values for the material parameters (τ , β , σ_0 , σ_∞) are depicted in Fig. 14.

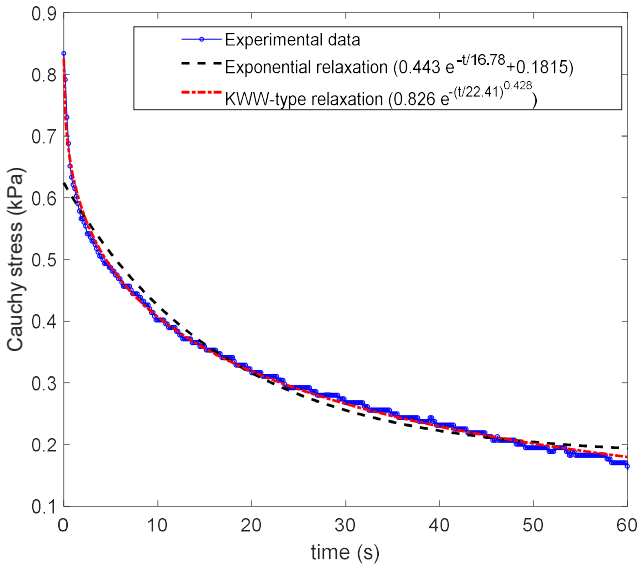

Fig. 14. The Cauchy stress versus time relation in the second step of the stress relaxation test of the GG 0.6% SPM specimen held in constant displacement for 60 seconds with the values for the material parameters (τ , β , σ_0 , σ_∞) employed in the simple decay exponential function and the stretched exponential KWW function. (22 N load cell in experiment and 1 Hz signal noise filtration)

In these figures, it can be seen that the stretched exponential KWW function allows a better fit to the stress relaxation behaviour of the tested specimens than when using the simple decay exponential function. In particular, the fit is better for the early stages of relaxation. Indeed, the KWW function can evaluate the non-linearity of the stress-relaxation behaviour of these hydrogels.

The values determined for the material parameters for two compositions with 1.1% and 0.6% SPM concentration are listed in Table 1. From Table 1, it can be seen that the relaxation time values τ are lower for the specimen of 1.1% SPM concentration in comparison with the other concentration, whereas the empirical exponent value β is higher for the specimen of 0.6% SPM concentration. The relaxation time is directly related to the material damping properties. In general terms, as τ decreases the internal damping tends to increase and vice versa. As a result, a greater aptitude to dissipate or absorb the energy

of mechanical work occurs. The β term in the KWW stretched-exponential characterises the degree of non-exponentially of the relaxation function. Generally, the distribution changes from a broad distribution to a sharp one, increasing β from 0 to 1. Moreover, the relaxation distribution is sharper for the specimen of 0.6% SPM concentration with a higher value for the empirical exponent.

Table 1. Fitted values of the material parameters by simple decay exponential and KWW-type function for different compositions of GG hydrogel.

hydrogel	model	τ	β	σ_0 (kPa)	σ_∞ (kPa)
GG 1.1% SPM	Simple decay Exponential	12.06	-	1.603	0.522
	KWW	11.48	0.391	3.031	-
GG 0.6% SPM	Simple decay Exponential	16.78	-	0.433	0.1815
	KWW	22.41	0.428	0.826	-

4.5 Artefacts affecting the compressive moduli determination

The stress-strain behaviour of hydrogel during simulated compression testing with various artefacts is shown in Fig. 15, and one example case is shown in Supplementary Video 4. The modelled 'artefacts' only produce essentially linear behaviour – the only exception being the model with a non-flat top geometry (specimen top-aligned 5°). The non-linearity produced by the initial partial contact to the specimen is merely an insignificant feature when noting the large, modelled alignment and the highly linear response after full contact with the (modelled) test machine surface. It should be noted, however, that the produced slope does not fully recover for the aligned specimen when compared to the response of the standard specimen with an ideal geometry. The important detail from the 3D simulations is the local stress concentration at the specimen corner (see Fig. 15 and 'worming' in Supplementary Video 4). The stress concentration requires either slippage or plastic or viscous flow in a real hydrogel specimen. Only at an ideal frictionless boundary, the stress concentration would not occur. Due to the real,

finite friction in a practical test environment, entirely elastic compression is impossible to produce over a large displacement (strain) range.

The dynamic simulations indicated that (1) the effects of inertia and kinetic energy are not crucial and that (2) immediate relaxation occurs during the compression testing at typical test rates. As presented in Fig. 16 and Supplementary Video 5, a presumed elastic (linear) behaviour cannot be produced by using the elastic constants fitted directly to the compression test due to relaxation. In other words, the experimental test output is not a representation of uniaxial elastic compression but a simultaneous relaxation and (visco) elastic deformation. Therefore, the modulus values anticipated in Eq. (5) are 'effective' constants for the elastic-dissipative behaviour after the 'first iteration'. For the GG hydrogel considered in this study, a test rate of at least 10 mm/min is necessary for an acceptable error in linearity due to the viscous effects (maximum logarithmic strain in the order of 5% to 10%). Higher accuracy can be reached by (1) focusing on the higher rate test data; (2) updating the (quasi) static compression models for the proper deformation region and (3) re-fitting the relaxation model based on the updated elastic region (at the beginning of a relaxation test).

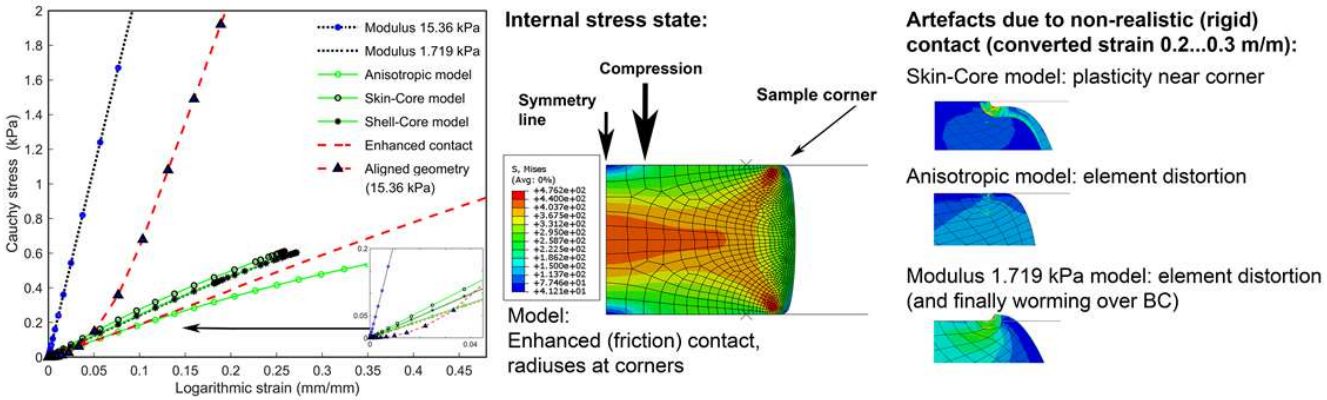

Fig. 15. FEA cases of presumed elastic test region with different artefacts of compression testing and material homogeneity. The stress and strain are calculated from the force and deformation output by using Eqs. (3) and (4).

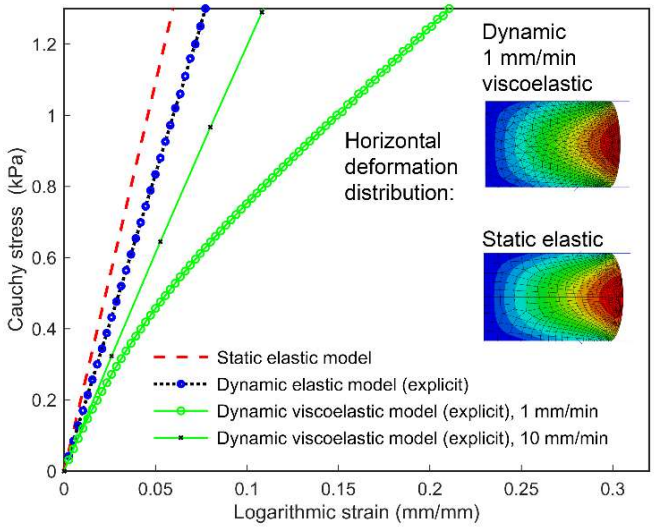

Fig. 16. FEA cases of hydrogel compression with a fully elastic model (implicit), a model with dynamic effects considered and a model with dynamic and viscoelastic (relaxation) behaviour simulated. The stress and strain are calculated from the force and deformation output by using Eqs. (3) and (4).

4.6. Procedure for determining hydrogel compressive modulus

The following is the suggested procedure for hydrogel compression testing to determine elastic compressive modulus:

- Select a displacement rate-range where no significant leaking of water from the hydrogel specimen or any visible permanent deformation is observed.
- Specimen size should be measured individually for each compression specimen due to possible variations in the hydrogel production (geometry). Specimen height should be low enough to rule out bending and buckling.
- Specimen slippage can be minimised by adding a small piece of wet lint-free cellulose paper on both compression anvils. This increases friction between the hydrogel and machine. Although this makes the measurement easier, it causes the stress field to be clearly non-uniaxial on the edges of the specimen. The paper should be replaced after each test to ensure similar friction for each specimen.
- Care should be taken in adjusting the starting point of the measurement so as not to apply any unknown pre-load that could obscure a possible ‘toe’ region in the raw test data.

- Compute the Cauchy stress and logarithmic strain as given in Eqs. (3) and (4) and Fig. 5.
- The first estimated stress-strain curve might be characterised by an (exponential) toe region followed by an essentially linear portion. A continuous method introduced here can be used to fit both portions simultaneously. In this event, a stress-strain model can be defined by the three parameters p and the constants A and B (see Eq. (5)) to compare different specimens.
- Perform a relaxation test in compression per hydrogel type. Select a suitable model to fit the constants, such as τ , β , σ_0, of the KWW stretched exponential function.

- Simulate the compression test using a modelling technique (e.g., with FEM implementation) that simultaneously computes the elastic deformation and (rate-dependent) degradation with the parameters (constants) determined by the experiments. Determine the 'elastic region' in terms of test rate and level of deformation (strain) with a selected maximum error (e.g., <20% exaggerated modulus).

- Iterate the above experimental-numerical cycle until the value of modulus (moduli) converge (error convergence depends on the originally selected stress-strain data and their shape).

In future, this method should be used to characterise different hydrogel compositions, produced using different crosslinking methods, to be able to truly compare the elastic behaviour of hydrogels (at a comparable level of accuracy). The time-consuming iteration for the compressive modulus has the advantage that it also results in the characterised dissipative (e.g., viscous) behaviour of the hydrogel specimens.

In this study, the displacement rates (e.g., 1 mm/min and 10 mm/min) significantly affected the measured responses of hydrogel. Based on the relaxation data and FEA, the error in directly measuring the elastic response (by presuming stress has not relaxed) is 43% at a maximum of

0%-8% (logarithmic) strain data range and a test speed of 10 mm/min. For a test speed of 1 mm/min, the corresponding error is 63%. In terms of the estimated Young's modulus by least squares fitting, the errors are 21% (fitting quality R^2=0.9998) and 50% (fitting quality R^2=0.9896) for 10 mm/min and 1 mm/min, respectively, and when compared to the real modulus as it was inputted for FEA of the ideal elastic model. Due to the fast relaxation in the hydrogel of this study, minimising the strain range of Young's modulus fitting does not markedly improve the estimated modulus. It is clear, however, that the 10 mm/min or even higher test speed should be selected here. If the determined relaxation data is presumed to be valid, the true Young's modulus of the GG hydrogel with a 1.1% SPM concentration is 19.2 kPa. For a 0.6% SPM content, the true Young's modulus is 6.7 kPa for a similar estimation of relaxation during testing. In these values of true moduli, the 'second' portion of the stress-strain curve is considered, and the 'toe' region is excluded (more characterisation would be needed to validate the lowest force and displacement values).

It should be noted, however, that fast relaxation also affects the estimated stress in the first phase (compression) of the relaxation test. Therefore, the peak stress at the beginning of the relaxation phase is not exactly true when presuming elastic response (i.e., Eq. 11). Whenever extreme accuracy (in Young's modulus) is necessary, the relaxation data (e.g., relaxation modulus) should be re-iterated (e.g., by FEA capable of simultaneous elastic and viscous/dissipative response). In general, the testing of hydrogels for exact viscous/dissipative behaviour (data) should be further developed in future, e.g., in terms of improved relaxation or creep testing.

Conclusions

In this paper, a specific approach to characterise the mechanical compressive response of hydrogels with a proper set of material parameters and analysis is proposed. Hydrogels have a nonlinear and dissipative behaviour when subject to mechanical loading. A continuous method is therefore introduced to fit both the exponential and linear portions of stress-strain data

simultaneously, which ensures continuity in the data analysis. The continuous method provides an improved fit to the test data, leading to a precise basis for dividing the data into different behaviour. The data analysis is continued to cover the determining of a stress relaxation response that can be modelled using a KWW-type model. Throughout the testing, the stress and strain values are expressed as Cauchy stress and logarithmic strain and confirmed by 3D-DIC imaging of deformation. Finally, the presumed elastic portions used for determining (Young's) modulus are corrected to exclude the error due to viscous (dissipative) relaxation. To present the performance and utility of the proposed approach, it is applied to two different compositions of bioamine crosslinked gellan gum hydrogel at two displacement test rates. The proposed method should be used in future for a more thorough and representative mechanical characterisation of both TE scaffold materials and target tissues, providing a better understanding of the requirements of manufacturing mechanically biomimicking biomaterials. Here, the approach indicates an error of between 21% and 50% when no relaxation is accounted for. After correcting for viscous relaxation, Young's moduli of ≈19 kPa and ≈7 kPa are determined for 1.1% and 0.6% SPM contents, respectively.

Acknowledgements

J.T. Koivisto and M. Kellomäki would like to thank the Human Spare Parts program of Business Finland for the funding of this research. J.T. Koivisto would also like to acknowledge the support given by the Finnish Cultural Foundation the Pirkanmaa Regional Fund personal grant number 50151501. J. Nafar Dastgerdi, O. Orell and M. Kanerva would like to thank the 'LuxTurrim5G' project grant by Business Finland and the related subtask (10098/31/2016) about compression testing of polymers and polymer composites carried out by Tampere University of Technology. The authors wish to thank Peter Heath for help with language checking and proof-reading the manuscript. CSC–IT Center for Science (Finland) is acknowledged for computational resources.

Electronic supplementary information

Video 1 shows an example of the GG 1.1% SPM hydrogel compression test with displacement rate of 10 mm/min. Videos 2A and 3 show the behaviour of the GG 1.1% SPM hydrogel samples during compression using new papers and papers used several times, i.e., varied friction, between the sample and the compression plates. Video 2B shows the analysed strain as a heat map. Videos 4 (implicit FEA for the elastic model) and 5 (explicit FEA for the dynamic model) illustrate the simulated compression with the effect of sliding at the machine-sample boundary. Video 5A shows the full sample, and 5B is zoomed in on the upper part of the sample.

References

[1] S.J. Buwalda, K.W.M. Boere, P.J. Dijkstra, J. Feijen, T. Vermonden, W.E. Hennink, Hydrogels in a historical perspective: From simple networks to smart materials, J. Control. Release. 190 (2014) 254–273. https://doi.org/10.1016/j.jconrel.2014.03.052.

[2] S.H. Aswathy, U. Narendrakumar, I. Manjubala, 2020. Commercial hydrogels for biomedical applications, Heliyon,. 6, e03719, https://doi.org/10.1016/j.heliyon.2020.e03719.

[3] X. Zhang, P. Huang, G. Jiang, M. Zhang, F. Yu, X. Dong, L. Wang, Y. Chen, W. Zhang, Y. Qi, W. Li, H. Zeng, 2021. A novel magnesium ion-incorporating dual-crosslinked hydrogel to improve bone scaffold-mediated osteogenesis and angiogenesis, Mater. Sci. Eng. C. 121, 111868. https://doi.org/10.1016/j.msec.2021.111868.

[4] J. Li, D.J. Mooney, 2016. Designing hydrogels for controlled drug delivery, Nat. Rev. Mater. 1, 16071. https://doi.org/10.1038/natrevmats.2016.71.

[5] B.G. Chung, K.-H. Lee, A. Khademhosseini, S.-H. Lee, Microfluidic fabrication of microengineered hydrogels and their application in tissue engineering, Lab Chip. 12 (2011) 45–59. https://doi.org/10.1039/C1LC20859D.

[6] M.E. Gomes, M. Rodrigues, R.M.A. Domingues, R.L. Reis, Tissue Engineering and Regenerative Medicine: New Trends and Directions—A Year in Review, Tissue Eng. Part B Rev. 23 (2017) 211–224. https://doi.org/10.1089/ten.teb.2017.0081.

[7] S. Breslin, L. O'Driscoll, Three-dimensional cell culture: The missing link in drug discovery, Drug Disc. Today, 18 (2013) 240–249. https://doi.org/10.1016/j.drudis.2012.10.003.

[8] S.B. Shah, A. Singh, Cellular self-assembly and biomaterials-based organoid models of development and diseases, Acta Biomater. 53 (2017) 29–45. https://doi.org/10.1016/j.actbio.2017.01.075.

[9] A.J. Engler, S. Sen, H.L. Sweeney, D. E. Discher, Matrix Elasticity Directs Stem Cell Lineage Specification, Cell. 126 (2006) 677–689. https://doi.org/10.1016/j.cell.2006.06.044.

[10] W.L. Murphy, T.C. McDevitt, A.J. Engler, Materials as stem cell regulators, Nat. Mater. 13 (2014) 547–557. https://doi.org/10.1038/nmat3937.

[11] N.J. Walters, E. Gentleman, Evolving insights in cell-matrix interactions: Elucidating how non-soluble properties of the extracellular niche direct stem cell fate, Acta Biomater. 11 (2015) 3–16. https://doi.org/10.1016/j.actbio.2014.09.038.

[12] F. Brandl, F. Sommer, A. Goepferich, Rational design of hydrogels for tissue engineering: Impact of physical factors on cell behavior, Biomaterials. 28 (2007) 134–146. https://doi.org/10.1016/j.biomaterials.2006.09.017.

[13] F.M. Watt, W.T.S. Huck, Role of the extracellular matrix in regulating stem cell fate, Nat. Rev. Mol. Cell Biol. 14 (2013) 467–473. https://doi.org/10.1038/nrm3620.

[14] S.K. Bhatia, Engineering Biomaterials for Regenerative Medicine: Novel Technologies for Clinical Applications, first ed., Springer New York, New York, 2012.

[15] A.M. Handorf, Y. Zhou, M.A. Halanski, W.-J. Li, Tissue stiffness dictates development, homeostasis, and disease progression, Organogenesis. 11 (2015) 1–15. https://doi.org/10.1080/15476278.2015.1019687.

[16] G. Mattei, A. Ahluwalia, Sample, testing and analysis variables affecting liver mechanical properties: A review, Acta Biomater. 45 (2016) 60–71. https://doi.org/10.1016/j.actbio.2016.08.055.

[17] R.K. Das, V. Gocheva, R. Hammink, O.F. Zouani, A.E. Rowan, Stress-stiffening-mediated stem-cell commitment switch in soft responsive hydrogels, Nat. Mater. 15 (2016) 318–325. https://doi.org/10.1038/nmat4483.

[18] C. Storm, J.J. Pastore, F.C. MacKintosh, T.C. Lubensky, P.A. Janmey, Nonlinear elasticity in biological gels, Nature. 435 (2005) 191–194. https://doi.org/10.1038/nature03521.

[19] A.V. Dobrynin, J.-M.Y. Carrillo, Universality in nonlinear elasticity of biological and polymeric networks and gels, Macromolecules. 44 (2011) 140–146. https//doi.org/10.1021/ma102154u.

[20] H. Hencky, Über die form des elastizitätsgesetzes bei ideal elastischen stoffen, Z. Techn. Phys. 9 (1928) 215–220.

[21] H. Xiao, O.T. Bruhns, A. Meyers, Explicit dual stress-strain and strain-stress relations of incompressible isotropic hyperelastic solids via deviatoric Hencky strain and Cauchy stress, Acta Mech. 168 (2004) 21–33. https://doi.org/10.1007/s00707-004-0074-5.

[22] H. Xiao, O.T. Bruhns, A. Meyers, Elastoplasticity beyond small deformations, Acta Mech. 182 (2006) 31–111. https://doi.org/10.1007/s00707-005-0282-7.

[23] R. Naghdabadi, M. Yeganeh, A.R. Saidi, Application of corotational rates of the logarithmic strain in constitutive modeling of hardening materials at finite deformations, Int. J. Plast. 21 (2005) 1546–1567. https://doi.org/10.1016/j.ijplas.2004.07.005.

[24] R.C. Lin, U. Schomburg, A novel internal dissipation inequality by isotropy and its implication for inelastic constitutive characterization, Mech. Res. Commun. 30 (2003) 125–133. https://doi.org/10.1016/S0093-6413(02)00349-X.

[25] M.L. Oyen, Mechanical characterisation of hydrogel materials, Int. Mater. Rev. 59 (2014) 44–59. https://doi.org/10.1179/1743280413Y.0000000022.

[26] F. Hild, S. Roux, Digital image correlation: From displacement measurement to identification of elastic properties – a review, Strain. 42 (2006) 69–80. https://doi.org/10.1111/j.1475-1305.2006.00258.x.

[27] H. Schreier, J.-J. Orteu, M.A. Sutton, Image Correlation for Shape, Motion and Deformation Measurements. first ed., Springer US, New York, 2009.

[28] M. Palanca, G. Tozzi, L. Cristofolini, The use of digital image correlation in the biomechanical area: A review, Int. Biomech. 3 (2016) 1–21. https://doi.org/10.1080/23335432.2015.1117395.

[29] J.L. Drury, R.G. Dennis, D.J. Mooney, The tensile properties of alginate hydrogels, Biomaterials. 25 (2004) 3187–3199. https://doi.org/10.1016/j.biomaterials.2003.10.002.

[30] J.D. Ferry, Viscoelastic Properties of Polymers, third ed., John Wiley & Sons, New York, 1980.

[31] X. Zhao, N. Huebsch, D.J. Mooney, Z. Suo, 2010. Stress-relaxation behavior in gels with ionic and covalent crosslinks. J. Appl. Phys. 107, 063509. https://doi.org/10.1063/1.3343265.

[32] S.A. Chester, A constitutive model for coupled fluid permeation and large viscoelastic deformation in polymeric gels, Soft Matter. 8 (2012) 8223–8233. https://doi.org/10.1039/C2SM25372K.

[33] R. Bai, J. Yang, Z. Suo, Fatigue of hydrogels, Eur. J. Mech. A Solids. 74 (2019) 337–370. https://doi.org/10.1016/j.euromechsol.2018.12.001.

[34] A. Bauer, L. Gu, B. Kwee, W.A. Li, M. Dellacherie, A.D. Celiz, D.J. Mooney, Hydrogel substrate stress-relaxation regulates the spreading and proliferation of mouse myoblasts, Acta Biomater. 62 (2017) 82–90. https://doi.org/10.1016/j.actbio.2017.08.041.

[35] R. Kocen, M. Gasik, A. Gantar, S.S. Novak, 2017. Viscoelastic behavior of hydrogel-based composites for tissue engineering under mechanical load, Biomed. Mater. 12, 25004. https://doi.org/10.1088/1748-605x/aa5b00.

[36] O. Chaudhuri, Viscoelastic hydrogels for 3D cell culture, Biomater. Sci. 5 (2017) 1480–1490. https://doi.org/10.1039/C7BM00261K.

[37] K. Nakamura, E. Shinoda, M. Tokita, The influence of compression velocity on strength and structure for gellan gels, Food Hydrocoll. 15 (2001) 247–252. https://doi.org/10.1016/S0268-005X(01)00021-2.

[38] I.V. Gofman, A.L. Buyanov, Unusual effect evidenced at the investigations of the mechanical behavior of composite hydrogels under cyclic compression, J. Mech. Behav. Biomed. Mater. 71 (2017) 238–243. https://doi.org/10.1016/j.jmbbm.2017.03.030.

[39] M.A. Biot, General theory of three-dimensional consolidation, J. Appl. Phys. 12 (1941) 155–164. https://doi.org/10.1063/1.1712886.

[40] W. Hong, X. Zhao, J. Zhou,, Z. Suo, A theory of coupled diffusion and large deformation in polymeric gels, J. Mech. Phys. Solids. 56 (2008) 1779–1793. https://doi.org/10.1016/j.jmps.2007.11.010.

[41] J. Yoon, S. Cai, Z. Suo, R.C. Hayward, Poroelastic swelling kinetics of thin hydrogel layers: Comparison of theory and experiment, Soft Matter. 6 (2010) 6004–6012. https://doi.org/10.1039/C0SM00434K.

[42] Y. Li, T. Tanaka, Kinetics of swelling and shrinking of gels, J. Chem. Phys. 92 (1990) 1365–1371. https://doi.org/10.1063/1.458148.

[43] M. Quesada-Pérez, J. Maroto-Centeno, J. Forcada, R. Hidalgo-Alvarez, Gel swelling theories: The classical formalism and recent approaches, Soft Matter. 7 (2011) 10536–10547. https://doi.org/10.1039/C1SM06031G.

[44] S. Cai, Y. Hu, X. Zhao, Z. Suo, 2010. Poroelasticity of a covalently crosslinked alginate hydrogel under compression, J. Appl. Phys. 108, 113514. https://doi.org/10.1063/1.3517146.

[45] W. Hong, Z. Liu, Z. Suo, Inhomogeneous swelling of a gel in equilibrium with a solvent and mechanical load, Int. J. Solids Struct. 46 (2009) 3282–3289. https://doi.org/10.1016/j.ijsolstr.2009.04.022.

[46] S. A. Chester, L. Anand, A coupled theory of fluid permeation and large deformations for elastomeric materials, J. Mech. Phys. Solids. 58 (2010) 1879–1906. https://doi.org/10.1016/j.jmps.2010.07.020.

[47] W. Hong, X. Zhao, Z. Suo, Large deformation and electrochemistry of polyelectrolyte gels, J. Mech. Phys. Solids. 58 (2010) 558–577. https://doi.org/10.1016/j.jmps.2010.01.005.

[48] M.K. Kang, R. Huang, A variational approach and finite element implementation for swelling of polymeric hydrogels under geometric constraints, J. Appl. Mech. 77 (2010) 61004–61012. https://doi.org/10.1115/1.4001715.

[49] A. Lucantonio, P. Nardinocchi, L. Teresi, Transient analysis of swelling-induced large deformations in polymer gels, J. Mech. Phys. Solids. 61 (2013) 205–218. https://doi.org/10.1016/j.jmps.2012.07.010.

[50] J. Zhang, X. Zhao, Z. Suo, H. Jiang, 2009. A finite element method for transient analysis of concurrent large deformation and mass transport in gels, J. Appl. Phys. 105, 93522. https://doi.org/10.1063/1.3106628.

[51] Q.-M. Wang, A.C. Mohan, M.L. Oyen, X.-H. Zhao, Separating viscoelasticity and poroelasticity of gels with different length and time scales, Acta Mech. Sin. 30 (2014) 20–27. https://doi.org/10.1007/s10409-014-0015-z.

[52] Y. Hu, Z. Suo, Viscoelasticity and poroelasticity in elastomeric gels, Acta Mech. Solida Sin. 25 (2012) 441–458. https://doi.org/10.1016/S0894-9166(12)60039-1.

[53] D. Caccavo, G. Lamberti, PoroViscoElastic model to describe hydrogels' behavior, Mater. Sci. Eng. C. 76 (2017) 102–113. https://doi.org/10.1016/j.msec.2017.02.155.

[54] X. Zhao, S.J.A. Koh, Z. Suo, Nonequilibrium thermodynamics of dielectric elastomers, Int. J. Appl. Mech. 3 (2011) 203–217. https://doi.org/10.1142/S1758825111000944.

[55] X. Wang, W. Hong, A visco-poroelastic theory for polymeric gels, Proc. Math. Phys. Eng. Sci. 468 (2012) 3824–3841. https://dx.doi.org/10.1098/rspa.2012.0385.

[56] D.T.N. Chen, Q. Wen, P.A. Janmey, J.C. Crocker, A.G. Yodh, Rheology of soft materials, Annu. Rev. Condens. Matter Phys. 1 (2010) 301–322. https://doi.org/10.1146/annurev-conmatphys-070909-104120.

[57] J. Yang, W. Illeperuma, Z. Suo, 2020. Inelasticity increases the critical strain for the onset of creases on hydrogels, Extreme Mech. Lett. 40, 100966. https://doi.org/10.1016/j.eml.2020.100966.

[58] Y.C. Fung, Elasticity of soft tissues in simple elongation, Am. J. Physiol. 213 (1967) 1532–1544. https://doi.org/10.1152/ajplegacy.1967.213.6.1532.

[59] A.H. Bacelar, J. Silva-Correia, J.M. Oliveira, R.L. Reis, Recent progress in gellan gum hydrogels provided by functionalization strategies, J. Mater. Chem. B. 4 (2016) 6164-6174. https://doi.org/10.1039/c6tb01488g.

[60] J.T. Koivisto, T. Joki, J.E. Parraga, R. Pääkkönen, L. Ylä-Outinen, L. Salonen, I. Jönkkäri, M. Peltola, T.O. Ihalainen, S. Narkilahti, M. Kellomäki, 2017. Bioamine-crosslinked gellan gum hydrogel for neural tissue engineering, Biomed. Mater. 12, 025014. https://doi.org/10.1088/1748-605X/aa62b0.

[61] J. Karvinen, J.T. Koivisto, I. Jönkkäri, M. Kellomäki, The production of injectable hydrazone crosslinked gellan gum-hyaluronan-hydrogels with tunable mechanical and physical properties, J. Mech. Behav. Biomed. Mater. 71 (2017) 383–391. https://doi.org/10.1016/j.jmbbm.2017.04.006.

[62] J.T. Koivisto, C. Gering, J. Karvinen, R. Maria Cherian, B. Belay, J. Hyttinen, K. Aalto-Setälä, M. Kellomäki, J. Parraga, Mechanically biomimetic gelatin–gellan gum hydrogels for 3D culture of beating human cardiomyocytes, ACS Appl. Mater. Interfaces. 11 (2019) 20589–20602. https://doi.org/10.1021/acsami.8b22343.

[63] C. Gering, J.T. Koivisto, J.E. Parraga, M. Kellomäki, Reproducible preparation method of hydrogels for cell culture applications – Case study with spermidine crosslinked gellan gum, IFMBE Proc. 65 (2017) 811-814. https://doi.org/10.1007/978-981-10-5122-7_203.

[64] Y.-C. Fung, Biomechanics: Mechanical Properties of Living Tissues, first ed., Springer-Verlag, New York, 1981.

[65] A.Ya. Malkin, Rheology Fundamentals, first ed., ChemTec Publishing, Toronto-Scarborough, 1994.

[66] K.L. Ngai, Relaxation and diffusion in complex systems, first ed., Springer Science & Business Media, New York, 2011.

[67] G.G. Raju, Dielectrics in Electric Fields, first ed., CRC Press, Boca Raton, 2003.

[68] Y. Gueguen, V.Keryvin, T. Rouxel, M. Le Fur, H. Orain, B. Bureau, C. Boussard-Plédel, J.-C. Sangeleboeuf, A relationship between non-exponential stress relaxation and delayed elasticity in the viscoelastic process in amorphous solids: Illustration on a chalcogenide glass, Mech. Mater. 85 (2015) 47–56. https://doi.org/10.1016/j.mechmat.2015.02.013.

[69] R.S. Anderssen S.A. Husain, R.J. Loy, The Kohlrausch function: properties and applications, ANZIAM J. 45 (2004) 800–816, https://doi.org/10.21914/anziamj.v45i0.924.

[70] D. Kytýř, T. Doktor, M. Adorna, M. Neuhauserova, J. Sleichrt, N. Fenclova, A. Gantar, S. Novak, Deformation behavior of gellan gum based scaffold Subjected to compression loading, Appl. Mech. Mater. 821 (2016) 665–670. https://doi.org/10.4028/www.scientific.net/AMM.821.665.

[71] D. Kytýř, P. Zlámal, P. Koudelka, T. Fíla, N. Krčmářová, I. Kumpová, D. Vavřík, A. Gantar, S. Novak, Deformation analysis of gellan-gum based bone scaffold using on-the-fly tomography, Mater. Des. 134 (2017) 400–417. https://doi.org/10.1016/j.matdes.2017.08.036.

[72] J. Tang, M.A. Tung, Y. Zeng, Compression strength and deformation of gellan gels formed with mono- and divalent cations, Carbohydr. Polym. 29 (1996) 11–16. http://dx.doi.org/10.1016/0144-8617(95)00124-7.

[73] L. Koivusalo, J. Karvinen, E. Sorsa, I. Jönkkäri, J. Väliaho, P. Kallio, T. Ilmarinen, S. Miettinen, H. Skottman, M. Kellomäki, Hydrazone crosslinked hyaluronan-based hydrogels for therapeutic delivery of adipose stem cells to treat corneal defects, Mater. Sci. Eng. C. 85 (2018) 68-78. https://doi.org/10.1016/j.msec.2017.12.013.

[74] M. Dehghan-Niri, E. Vasheghani-Farahani, M. Baghaban Eslaminejad, M. Tavakol, F. Bagheri, 2020. Physicomechanical, rheological and in vitro cytocompatibility properties of the electron beam irradiated blend hydrogels of tyramine conjugated gum tragacanth and poly (vinyl alcohol), Mater. Sci. Eng. C. 114, 111073. https://doi.org/10.1016/j.msec.2020.111073.

[75] K. Vuornos, M. Ojansivu, J.T. Koivisto, H. Häkkänen, B. Belay, T. Montonen, H. Huhtala, M. Kääriäinen, L. Hupa, M. Kellomäki, J. Hyttinen, J.A. Ihalainen, S. Miettinen, Bioactive glass ions induce efficient osteogenic differentiation of human adipose stem cells encapsulated in gellan gum and collagen type I hydrogels, Mater. Sci. Eng. C. 99 (2019) 905-918. https://doi.org/10.1016/j.msec.2019.02.035.

[76] Y.R. Zhang, K.J. Xu, Y.L. Bai, L.Q. Tang, Z.Y. Jiang, Y.P. Liu, Z.J. Liu, L.C. Zhou, X.F. Zhou, Features of the volume change and a new constitutive equation of hydrogels under uniaxial compression, J. Mech. Behav. Biomed. Mater. 85 (2018) 181-187. https://doi.org/10.1016/j.jmbbm.2018.06.004.

[77] L.A. Pruitt, A.M. Chakravartula, Mechanics of Biomaterials - Fundamental Principles for Implant Design, first ed., Cambridge University Press, Cambridge, 2011.

[78] E. Gentleman, G.A. Livesay, K C. Dee, E.A. Nauman, Development of ligament-like structural organization and properties in cell-seeded collagen scaffolds in vitro, Ann. Biomed. Eng. 34 (2006) 726–736. https://doi.org/10.1007/s10439-005-9058-4.

[79] M.D. Shoulders, R.T. Raines, Collagen structure and stability, Annu. Rev. Biochem. 78 (2009) 929–958. https://doi.org/10.1146/annurev.biochem.77.032207.120833.

[80] R. Chandrasekaran, A. Radha, Molecular architectures and functional properties of gellan gum and related polysaccharides, Trends Food Sci. Technol. 6 (1995) 143–148. http://dx.doi.org/10.1016/S0924-2244(00)89022-6.

[81] S. Lee, W.G. Knauss, A note on the determination of relaxation and creep data from ramp tests, Mech. Time Depend. Mater. 4 (2000) 1–7. https://doi.org/10.1023/A:1009827622426.

Appendix

The anisotropic behaviour of hydrogels could stem from molecular stretching as a compression sample stretches horizontally. For a cylindrical test sample, the circumferential dimension likewise stretches according to the Poisson's ratios set. In the event of instantaneous stretching, the resulting elastic constants can be modelled by using engineering constants per direction. For an axisymmetric space with unit axes (directions) of Z, R, θ (i.e., axial, radial, circumferential), the constants in this study were estimated as follows:

$$E_\theta = 15360 \text{ Pa} \quad \text{(A1)}$$

$$E_Z = 1719 \text{ Pa}, \quad \text{(A2)}$$

where the stiffer behaviour (15.36 kPa) observed during the experiments is presumed to be due to a high modulus (E_θ) in the circumferential stretching direction of the cylindrical test sample. Likewise, the lower stiffness (the very initial toe region) is presumed to be due to a low modulus (E_Z) in the axial direction. The radial direction was presumed to act as the axial direction ($E_Z = E_R$) as in orthotropic material.

For hydrogel, being nearly fluid (incompressible), the Poisson's ratios were set as follows:

$$\nu_{ZR} = 0.48 \approx 0.5 \quad \text{(A3)}$$

and

$$\nu_{R\theta} = 0.48 \cdot \frac{E_R}{E_\theta} = 0.05. \quad \text{(A4)}$$

To preserve requirements (see e.g., [1]):

$$1 - \nu_{ij}\nu_{ji} > 0 \quad \text{(A5)}$$

and

$$|\nu_{ij}| < \sqrt{\frac{E_j}{E_i}} \quad \text{(A6)}$$

the value of $\nu_{Z\theta}$ was set to 0.03. Therefore, the Poisson's ratios satisfy:

$$1 - \nu_{ZR}\nu_{RZ} - \nu_{R\theta}\nu_{\theta R} - \nu_{Z\theta}\nu_{\theta Z} - 2 \cdot \nu_{ZR}\nu_{R\theta}\nu_{\theta Z} > 0\ . \quad \text{(A7)}$$

The shear moduli were calculated based on the relationship

$$G_{ij} = \frac{E_j}{2(1+\nu_{ij})}\ . \quad \text{(A8)}$$

Thus, that the following values were used in this study:

$G_{Z\theta} = 5.20$ kPa

$G_{ZR} = 0.58$ kPa

$G_{R\theta} = 7.29$ kPa.

References

[1] B.M. Lempriere, Poisson's ratio in orthotropic materials, AIAA J. 6 (1968) 2226–2227. https://doi.org/10.2514/3.4974.